Journal of Solid State Chemistry **142,** 382–392 (1999)
Article ID jssc.1998.8053, available online at http://www.idealibrary.com on IDEAL®

# Synthesis and Activation of Co–Mg–Al Layered Double Hydroxides

Solange Ribet, Didier Tichit,[1] Bernard Coq, Bernard Ducourant,* and Françoise Morato*

*Laboratoire de Matériaux Catalytiques et Catalyse en Chimie Organique U.M.R. 5618, C.N.R.S./E.N.S.C.M. 8, rue de l'Ecole Normale 34296 Montpellier Cedex 5, France; and *Laboratoire des Agrégats Moléculaires et Matériaux Inorganiques UPRESA 5072, Université Montpellier II, Place Eugène Bataillon 34095 Montpellier Cedex 5, France*

Received May 26, 1998; in revised form October 2, 1998; accepted October 6, 1998

**Several Co/Mg/Al layered double hydroxides (LDH) with $(Mg^{2+}+Co^{2+})/Al^{3+} = 2$ and 3 and $Mg^{2+}/Co^{2+}$ ranging from 0 to 4 have been synthesized by coprecipitation at pH = 9 and $NO_3^-$ as main compensating anions. All samples present well-crystallized layered structures. From the evolution of the lattice *a* parameter with respectively the Al content and the $Mg^{2+}/(Mg^{2+}+Co^{2+})$ ratio, it could be concluded that $Mg^{2+}$, $Co^{2+}$, and $Al^{3+}$ belong to the same lattice, which is confirmed by X-ray diffraction (XRD), where no excess phases are detected. Distinct structures, related to the composition of the samples, are detected when calcination is performed up to 773 K. For the cobalt rich samples a spinel-like phase is formed whose amount decreases when the magnesium content increases. At high magnesium content a MgO-type phase is found. The thermal stabilities of intercalated $NO_3^-$ provided by the synthesis salts and of $CO_3^{2-}$ provided by the surrounding atmosphere increase with the magnesium content of the samples. Specific areas are also stabilized by Mg. TPR experiments provide evidence of two distinct reducible cobalt species whatever the sample. The species below 623 K are assigned to $Co_3O_4$. Those reduced around 970–1030 K must belong to a spinel-like phase whose composition largely depends on the Mg and Al content of the LDH. These two types of phases are quite indistinguishable by XRD due to their similar patterns.** 

## INTRODUCTION

Cobalt as a metal found applications in many important industrial catalytic processes, such as Fischer–Tropsch synthesis (1), hydrogenation of nitriles into amines (2), and reductive amination of alcohols (3). In supported catalysts, the reducibility of cobalt species often depends on the extent of metal–support interaction. It has been shown that cobalt reducibility became easier when changing the support from $SiO_2$ to $Al_2O_3$ and MgO or when the Al content increased in $SiO_2$–$Al_2O_3$ (4). A detailed temperature-programmed reduction (TPR) study provided evidence that four cobalt species would exist as a function of the reduction temperature of $Co/Al_2O_3$ (5). A high-temperature of calcination will favor the formation of a $Co^{2+}$–$Al^{3+}$ solid solution of spinel-type and of the stoichiometric $CoAl_2O_4$ spinel phase. Several species and particularly cobalt silicates were also detected by TPR in the case of $Co/SiO_2$ catalysts calcined at high temperature (6). These cobalt species in strong interaction with the support are generally inactive in hydrogenation due to their low reducibilities; their amounts depend largely on the type of the support. Moreover many parameters in the preparation, like the metal precursor, the nature of the solvent, and the aging time, influence the reducibility, the dispersion of the metals, and the nature of the crystalline phases (6). An interesting way to obtain mixed cobalt catalysts is through the use of layered double hydroxides (LDH), of the hydrotalcite-like family, as precursors (7, 8). They lead after calcination and reduction to small and stable metal crystallites. LDHs are anionic clays of the general formula

$$[M^{2+}_{1-x}M^{3+}_{x}(OH)_2]^{x+}(A^{m-})_{x/m},\quad nH_2O$$

with layers built up by condensation of octahedra whose $M^{2+}$ or $M^{3+}$ cations occupy the center and hydroxides ions the vertices. The cationic charges of the layers are compensated by hydrated anions in the interlayer space. These structures can also accommodate, simultaneously, several types of divalent and trivalent cations in the layers (7, 9). Their interest for catalytic applications arises from their ability to give mixed oxides of high specific surface area upon thermal treatments, inducing dehydroxylation of the layers and decomposition of the vaporizable anions (7, 10, 11). In a previous study (12), we used Ni/Mg/Al LDHs, with different Mg/Ni ratios, as precursors of catalysts for the hydrogenation of acetonitrile into amines. The metallic function was provided by

[1] To whom correspondence should be addressed. E-mail: tichit@cit.enscm.fr.



0022-4596/99 $30.00

reduction of $Ni^{2+}$ into Ni, while $Mg^{2+}$ was introduced with the aim to induce a basic character. It was indeed shown that:

(i) Co and Ni are the preferred metals for the primary amines formation (2, 13);

(ii) on tuning the acid-base character of the support, a change in selectivity should be found in favor of primary amines (12, 14, 15).

Several studies claimed that the support has a minor effect on the selectivity (2, 16).

From these observations we have decided to investigate the potential of Co/Mg/Al LDHs as precursors for hydrogenation catalysts. In the present study the synthesis of Co/Mg/Al LDHs with several cationic compositions will be presented. The as-prepared solids and those obtained at different stages of the activation, i.e., after treatments under oxidizing and reducing atmospheres, will be thoroughly investigated. Several observations have been reported concerning the crystallographic phases involved during the thermal decomposition of LDHs containing more than one divalent and/or trivalent cations, respectively. The nature of these cations and the temperature of activation induce the formation either of monophasic solid solutions with rock salt or spinel-like structures, or of a marked segregation of several phases (7). The $Co^{2+}/Al^{3+}$ and $Mg^{2+}/Al^{3+}$ LDHs indeed behave differently for calcination temperatures up to 1073 K (8). The former lead to a spinel-like structure (17) when the latter has the rock salt-like structure. When Co, Mg, and Al are associated the formation of $Co_xMg_{1-x}Al_2O_4$ solid solutions with the spinel structure and with various cations distribution has been reported (18, 19). With the aim of exploring new routes to catalytic materials, the activation of LDHs has been studied with attention paid to the textural properties, the chemical and structural homogeneity, and the reducibility of Co species. These aspects were investigated as a function of cations compositions and calcination treatments. It was indeed already shown that the reducibility of the cations strongly depends on the stoichiometry of the catalysts obtained from the LDHs (12, 20, 21).

## EXPERIMENTAL

### *Preparation of the LDH Precursors*

The materials were synthesized by coprecipitation under low supersaturating conditions. A solution containing the metallic nitrate salts $Co(NO_3)_2, 6H_2O$, $Mg(NO_3)_2, 6H_2O$, and $Al(NO_3)_3, 9H_2O$ (Aldrich) dissolved in 250 $cm^3$ of deionized water in appropriate concentrations was delivered, at room temperature under air, into a polypropylene reactor by a chromatography-type pump at a constant flow of 1 $cm^3\ min^{-1}$. A second aqueous solution of 1 M NaOH (SdS) was fed by a pH-stat apparatus (718 STAT TITRINO, Metrohm). The careful control of flow maintained the pH during precipitation in the reactor at a constant value of ca. $9.0 \pm 0.2$. After the precipitation was complete the resulting suspension was aged at $373 \pm 5$ K for 15 h under stirring. The solid product was isolated by centrifugation, washed thoroughly with deionized water, and dried overnight at 353 K in an oven. Eight samples were synthesized following this procedure, by varying both the total content in divalent cations $M^{2+}/Al^{3+} = 2$ and 3, with $M^{2+} = Co^{2+} + Mg^{2+}$, and the ratio between the divalent cations $Mg^{2+}/Co^{2+} = 0$, 0.25, 1, and 4.

The Mg free samples were labeled CoAl2 and CoAl3, and the mixed Co/Mg/Al compounds were labeled Mg(1)CoAl2, designating a sample containing Mg, Co, and Al cations with $Mg^{2+}/Co^{2+} = 1$ and $M^{2+}/Al^{3+} = 2$.

### *Characterizations of Solids*

Chemical analyses of the samples were performed at the Service Central d'Analyse du C.N.R.S. (Solaize, France). The powder X-ray diffraction (XRD) patterns were recorded on a Philips instrument (40 kV, 20 mA) using Cu$K\alpha$ radiation ($\lambda = 0.15401$ nm). The $2\theta$ angle ranged from 6° to 70°. A monochromator was applied to avoid fluorescence phenomenon. Thermogravimetric (TG) experiments were carried out on a Setaram TG 85 1000°C microbalance under a flow of air (80 $cm^3\ min^{-1}$) at a heating rate of 2 K $min^{-1}$ from 293 to 973 K. Specific surface areas were determined by $N_2$ adsorption at 77 K with a Micromeritics ASAP 2000 instrument and using the BET equation. The samples were outgassed under vacuum ($2 \times 10^{-4}$ Pa) at 523 K overnight before $N_2$ adsorption. The calcination of the samples was carried out, either at 573 K or at 773 K, with a furnace in flowing air at a heating rate of 2 K $min^{-1}$. The final temperature was maintained for 5 h.

The reducibility of the samples was examined by TPR by hydrogen. The experimental setup was derived from that proposed classically (22). The detection was carried out with the thermal conductivity detector of a Shimadzu GC8 chromatograph. The experimental parameters were carefully selected to meet the recommendations of Monti and Baiker (23). An aliquot of the catalyst (20–30 mg) was activated first at 623 and 773 K for 4 h in air (ramp; 2 K $min^{-1}$; flow; 50 $cm^3\ min^{-1}$) and then cooled to room temperature. Air was replaced by helium (purity $> 99.995\%$); then helium was replaced by the reducing $H_2$/Ar gas (3/97 vol/vol, purity of both gases $> 99.995\%$). Heating was then started from 293 to 1293 K (ramp; 10 K $min^{-1}$; flow; 20 $cm^3\ min^{-1}$). For CoAl2 and Mg(4)CoAl2, the nature of the outflowing gases was identified with the help of a Balzers QSM421 mass spectrometer in a different setup, but according to the same experimental procedure.

## RESULTS

### *Chemical Composition and X-ray Diffraction of the Materials from Synthesis*

The compositions of the materials from synthesis are listed in Table 1. They have been derived from the elemental analyses for Co, Mg, Al, C, and N contents, and from thermogravimetric experiments for the amount of structural water. The determined Co/Mg/Al molar compositions are very close to the composition of the original solution, except for the Mg content, which is always slightly lower than expected. The interlayer ions are both $NO_3^-$, which come from precursor salts, and $CO_3^{2-}$, which come from the surrounding atmosphere. The excess of anionic charge observed in some samples could be accounted for by the presence of bicarbonate or neutral carbonate species weakly bonded to the surface of the crystals. The presence of a small amount of $Co^{3+}$ formed by oxidation of $Co^{2+}$ during synthesis could not, however, be excluded (24).

The XRD profiles of the uncalcined materials are shown in Fig. 1. All samples crystallized in a single phase, with the layered structure. The different typical peaks of the hydrotalcite-like compounds are present: sharp and symmetrical reflections for (003), (006), (110), (113) planes and broad and asymmetrical peaks for (012), (015), (018) planes. However, there is a difference in the intensities of the reflections from one sample to another, indicating different degrees of crystallinity or structural order when the cationic composition varies. The CoAl2 and CoAl3 samples, containing only $Co^{2+}$ and $Al^{3+}$ cations, present sharp and intense (00*l*) peaks reflecting a high stacking order along the *c* axis. The other reflections are broad or totally vanished. For the Mg containing samples, the general trend is an increase in the peak intensity, other than (00*l*), as the Mg content increases. The (110) and (113) reflections thus become intense and well defined on Mg(4)CoAl2 and Mg(4)CoAl3, which could mean that the ordering along the *c* direction decreases while it increases into the layers. Moreover the (00*l*) reflections remain better defined with $M^{2+}/Al^{3+} = 2$ (CoAl2, Mg(0.25)CoAl2, Mg(1)CoAl2, and Mg(4)CoAl2 samples).

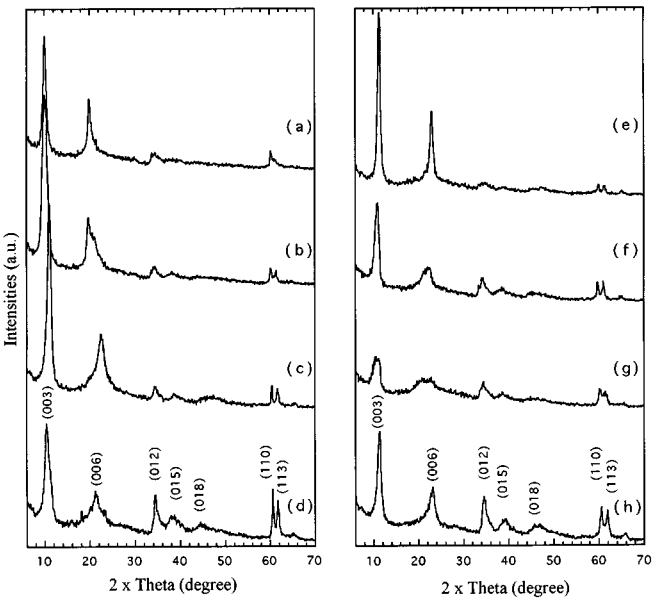


**FIG. 1.** X-ray diffraction patterns of the different samples: (a) CoAl2, (b) Mg(0.25)CoAl2, (c) Mg(1)CoAl2, (d) Mg(4)CoAl2, (e) CoAl3, (f) Mg(0.25)CoAl3, (g) Mg(1)CoAl3, (h) Mg(4)CoAl3.

The lattice *a* and *c* parameters, calculated using, respectively, the (110) and the (003) reflections and assuming a hexagonal structure, are listed in Table 1. Figure 2 shows that the lattice *a* parameter decreases when the $Mg^{2+}/(Mg^{2+} + Co^{2+})$ ratio goes on for the two series of samples with different Al molar fraction. This provides evidence that $Co^{2+}$ is substituted by $Mg^{2+}$ of smaller ionic radius. From this observation, we can deduce that in the range of compositions explored the $Co^{2+}$, $Mg^{2+}$, and $Al^{3+}$ cations belong to the same lattice of the hydrotalcite-like layers. This is confirmed by the absence of an additional phase or of a second hydrotalcite lattice in the XRD patterns.

**TABLE 1**
**Composition and Lattice Parameters of the Samples**

| Sample | Co:Mg:Al (at. ratio) | Chemical composition | *a* (nm) | *c* (nm) |
|---|---|---|---|---|
| CoAl2 | 2:0:1 | $[Co_{0.66}Al_{0.34}(OH)_2](CO_3^{2-})_{0.13}(NO_3^-)_{0.27}, 0.45H_2O$ | 0.3070 | 2.651 |
| CoAl3 | 3:0:1 | $[Co_{0.75}Al_{0.25}(OH)_2](CO_3^{2-})_{0.07}(NO_3^-)_{0.12}, 0.60H_2O$ | 0.3022 | 2.335 |
| Mg(0.25)CoAl2 | 1.6:0.4:1 | $[Co_{0.53}Mg_{0.13}Al_{0.34}(OH)_2](CO_3^{2-})_{0.13}(NO_3^-)_{0.21}, 0.44H_2O$ | 0.3074 | 2.544 |
| Mg(1)CoAl2 | 1:1:1 | $[Co_{0.31}Mg_{0.32}Al_{0.37}(OH)_2](CO_3^{2-})_{0.15}(NO_3^-)_{0.11}, 0.25H_2O$ | 0.3059 | 2.307 |
| Mg(4)CoAl2 | 0.4:1.6:1 | $[Co_{0.13}Mg_{0.53}Al_{0.36}(OH)_2](CO_3^{2-})_{0.13}(NO_3^-)_{0.17}, 0.35H_2O$ | 0.3055 | 2.448 |
| Mg(0.25)CoAl3 | 2.4:0.6:1 | $[Co_{0.62}Mg_{0.13}Al_{0.25}(OH)_2](CO_3^{2-})_{0.03}(NO_3^-)_{0.19}, 0.46H_2O$ | 0.3032 | 2.420 |
| Mg(1)CoAl3 | 1.5:1.5:1 | $[Co_{0.41}Mg_{0.32}Al_{0.27}(OH)_2](CO_3^{2-})_{0.04}(NO_3^-)_{0.19}, 0.56H_2O$ | 0.3080 | 2.447 |
| Mg(4)CoAl3 | 0.6:2.4:1 | $[Co_{0.18}Mg_{0.52}Al_{0.30}(OH)_2](CO_3^{2-})_{0.10}(NO_3^-)_{0.08}, 0.50H_2O$ | 0.3057 | 2.286 |

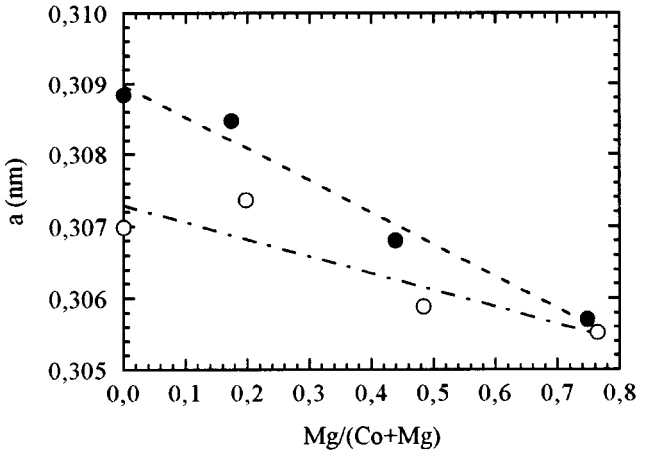


**FIG. 2.** Variation of the lattice *a* parameter of the samples as a function of the $Mg^{2+}/(Mg^{2+} + Co^{2+})$ ratio for $M^{2+}/Al^{3+} = 2$ (○) $M^{2+}/Al^{3+} = 3$ (●) samples.

*Activation under Air of the Materials from Synthesis*

The decomposition of the samples in air was followed by thermogravimetry in the 293 to 973 K temperature range. Moreover, for the CoAl2 and Mg(4)CoAl2 samples the nature of the gases released during the thermal treatment was monitored by mass spectrometry following the masses 18 ($H_2O$), 30 (NO, $NO_2$), 44 ($CO_2$), and 46 ($NO_2$). The representative TG and DTG curves of CoAl2, Mg(0.25)CoAl2, Mg(1)CoAl2, and Mg(4)CoAl2 are shown in Fig. 3. The total weight loss varied from 34 to 43% and exhibited from two to five steps when the Mg content increases. The most intense peak of the DTG profile shifted concurrently from 548 to 603 K. The comparison between TG (Fig. 3) and mass spectrometry (MS, Fig. 4) experiments shows that the first weight loss for CoAl2 (8% at 400 K) corresponds to the evolution of $H_2O$ alone. A similar behavior occurred for Mg(4)CoAl2, for which the first weight loss (13%) was accounted for $H_2O$ alone, too, but in a wider range of temperatures, from 350 to 520 K. These releases below 570 K are due to $H_2O$ differently bonded to the exchangeable anions in the interlayer space. The weight losses between 523 and 673 K (Fig. 4) correspond to $H_2O$ release due to the dehydroxylation of the layers and accompanied by evolution of $CO_2$ (mass 44) from $CO_3^{2-}$ and NO (mass 30) from $NO_3^-$; only trace amounts of $NO_2$ (mass 46) were detected. It is worth noting that $CO_2$ and NO were concurrently released at 523 K for CoAl2 , while NO was released at a higher temperature than $CO_2$ in Mg(4)CoAl2. This last material gave a tailing peak of $H_2O$ evolution with a maximum at 563 K, with the distinct release of NO under the tail. The slight shift between the temperatures of decomposition of the anions in the MS and TG experiments likely comes from the different setup used.

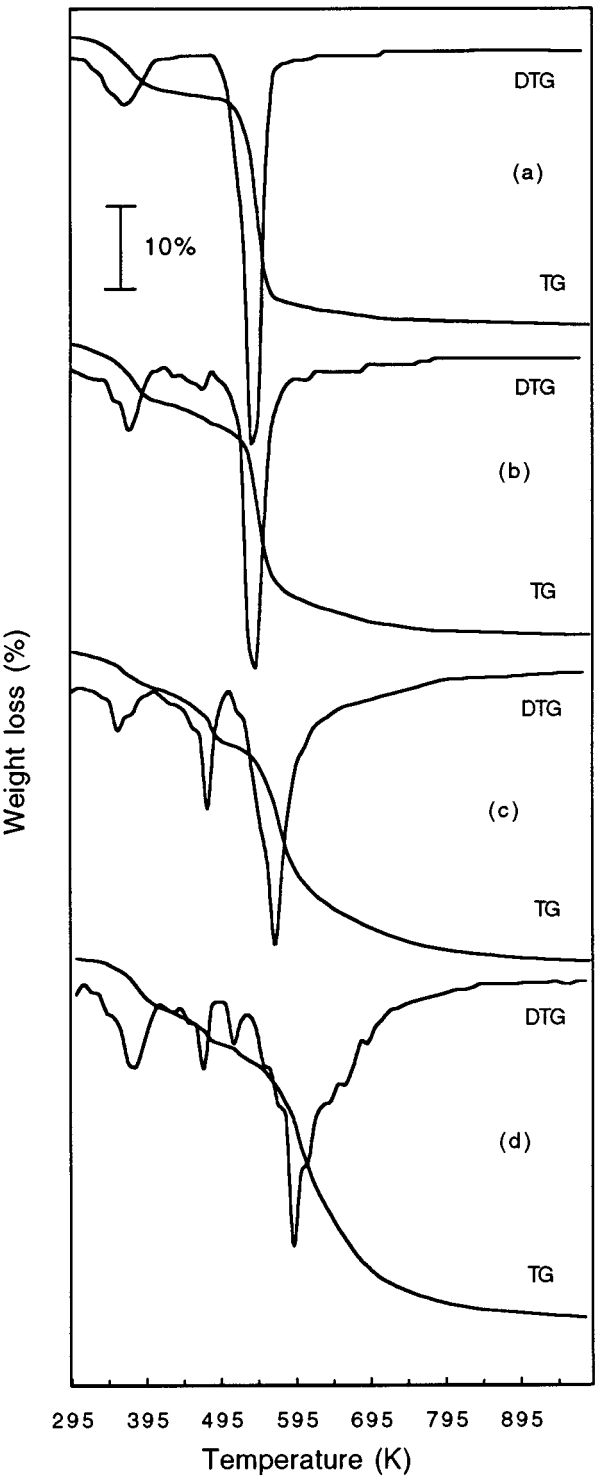


**FIG. 3.** TG–DTG profiles of the different samples: (a) CoAl2, (b) Mg(0.25)CoAl2, (c) Mg(1)CoAl2, (d) Mg(4)CoAl2.

The XRD patterns of the samples calcined at 573 and 773 K are reported in Figs. 5 and 6, respectively. After calcination at 573 K, only the (003) peaks of the hydrotalcite-like phases are still detected, but with a very low

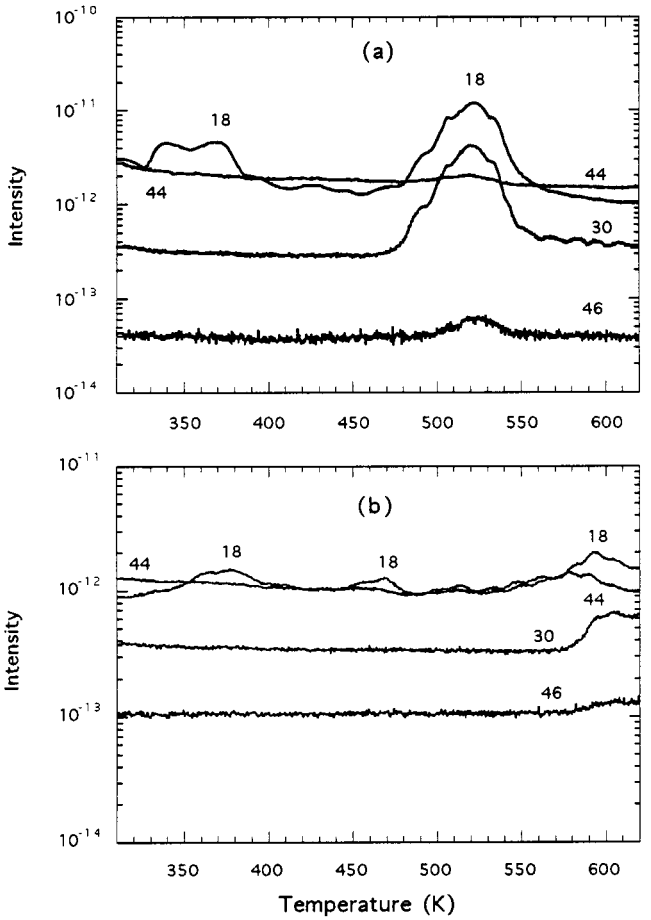


**FIG. 4.** Temperature-programmed decomposition followed by mass spectrometry of (a) CoAl2 and (b) Mg(4)CoAl2.

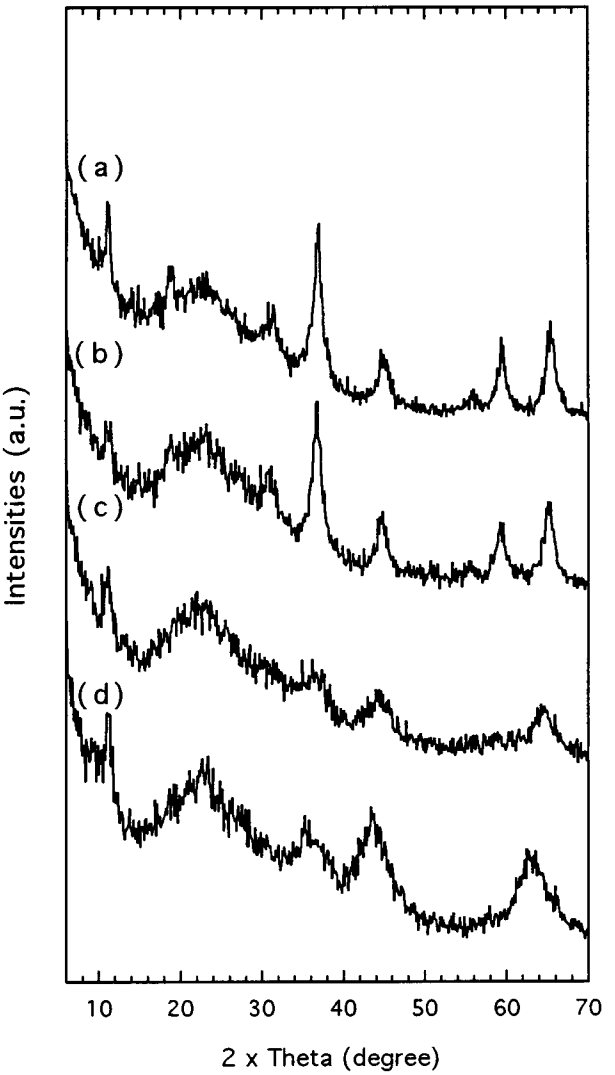


**FIG. 5.** X-ray diffraction patterns of the samples calcined at 573 K: (a) CoAl2; (b) Mg(0.25)CoAl2, (c) Mg(1)CoAl2, (d) Mg(4)CoAl2.

intensity. Great changes in the patterns occur with the chemical compositions. A phase assigned to a spinel-like structure gives intense lines in CoAl2 and CoAl3 samples. As the Mg content increases these lines are broadened, while those of a mixed oxide phase of the MgO type appear for Mg(1)CoAl2 and Mg(1)CoAl3. This latter phase, poorly crystallized, was the only one detected at the highest Mg content, i.e., in Mg(4)CoAl2 (Fig. 6d). After calcination at 773 K of every sample, the hydrotalcite-like structure is no longer detected. The peaks attributed to the spinel phase become narrower, while those of MgO-type phase remain comparatively broader. Therefore, these studies show that under calcination at 573 K, the hydrotalcite lattice of CoAl2 and CoAl3 is transformed into a well-crystallized $CoAl_2O_4$ spinel structure (Fig. 6a), as reported elsewhere (17). For the mixed $Mg^{2+}/Co^{2+}/Al^{3+}$ samples the behavior depends on the composition. As the Mg/Co ratio increases, the amount of spinel phase decreases as expected, but with a parallel decrease of crystallinity.

The specific surface areas of the materials after calcination at 573 and 773 K are given in Table 2. They range from 80 to 250 $m^2\,g^{-1}$ and culminate generally after calcination at 573 K, with a small decrease at both higher temperature and Mg content. The samples exhibit type II $N_2$ adsorption isotherms, following the BET classification (Fig. 7). On the other hand, the desorption isotherms are of type H4 for CoAl2 and of type H1 for Mg containing samples. This provides evidence that the pore shape moves from that characteristic of a lamellar structure to that with tubular capillaries (25). It should be pointed out that the calcination temperature did not affect the shape of either adsorption or desorption isotherms. The influence of both Mg content and temperature of calcination on the total surface area and the extent of microporosity, expressed as the specific surface area in pores smaller than 2 nm, are reported in Figs. 8 and 9, respectively. One can remark that the gap between the total surface area of the samples calcined at 573 and 773 K

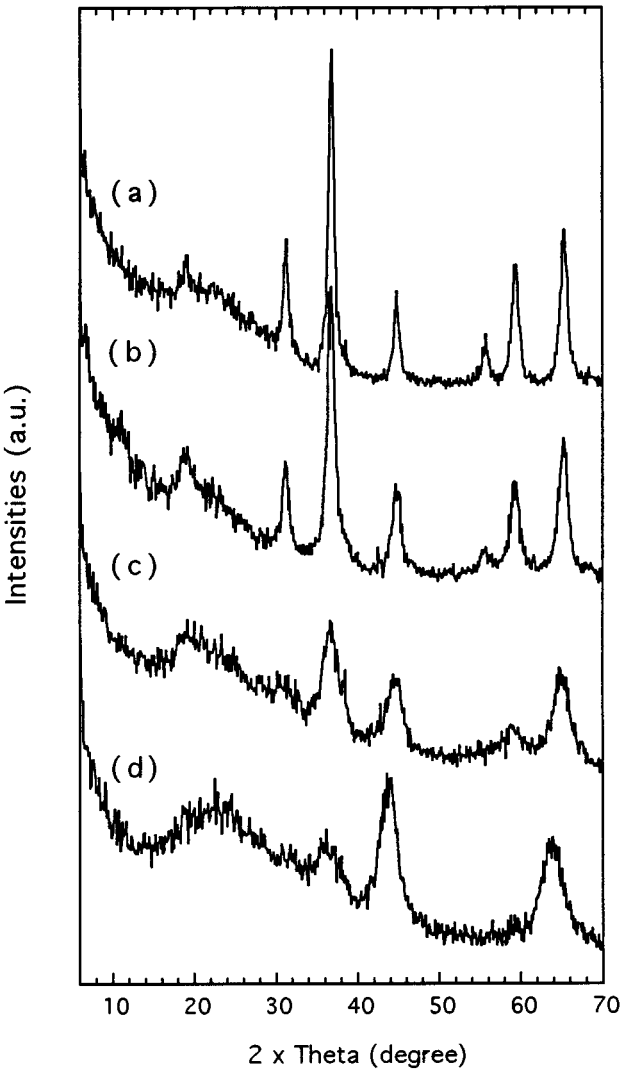


**FIG. 6.** X-ray diffraction patterns of the samples calcined at 773 K: (a) CoAl2; (b) Mg(0.25)CoAl2, (c) Mg(1)CoAl2, (d) Mg(4)CoAl2.

tends to reduce as the Mg content in the samples increases. They become thus almost similar for Mg(4)CoAl3 and Mg(4)CoAl2. This is likely due to a stabilizing effect of Mg.

**TABLE 2**
**Specific Surface Area of the Samples Calcined at 573 and 773 K**

| Sample | Co:Mg:Al (at. ratio) | Surface area ($m^2 g^{-1}$) | |
|---|---|---|---|
| | | 573 K | 773 K |
| CoAl2 | 2:0:1 | 158 | 82 |
| CoAl3 | 3:0:1 | 166 | 145 |
| Mg(0.25)CoAl2 | 1.6:0.4:1 | 181 | 133 |
| Mg(1)CoAl2 | 1:1:1 | 268 | 200 |
| Mg(4)CoAl2 | 0.4:1.6:1 | 242 | 249 |
| Mg(0.25)CoAl3 | 2.4:0.6:1 | 178 | 102 |
| Mg(1)CoAl3 | 1.5:1.5:1 | 177 | 146 |
| Mg(4)CoAl3 | 0.6:2.4:1 | 233 | 242 |

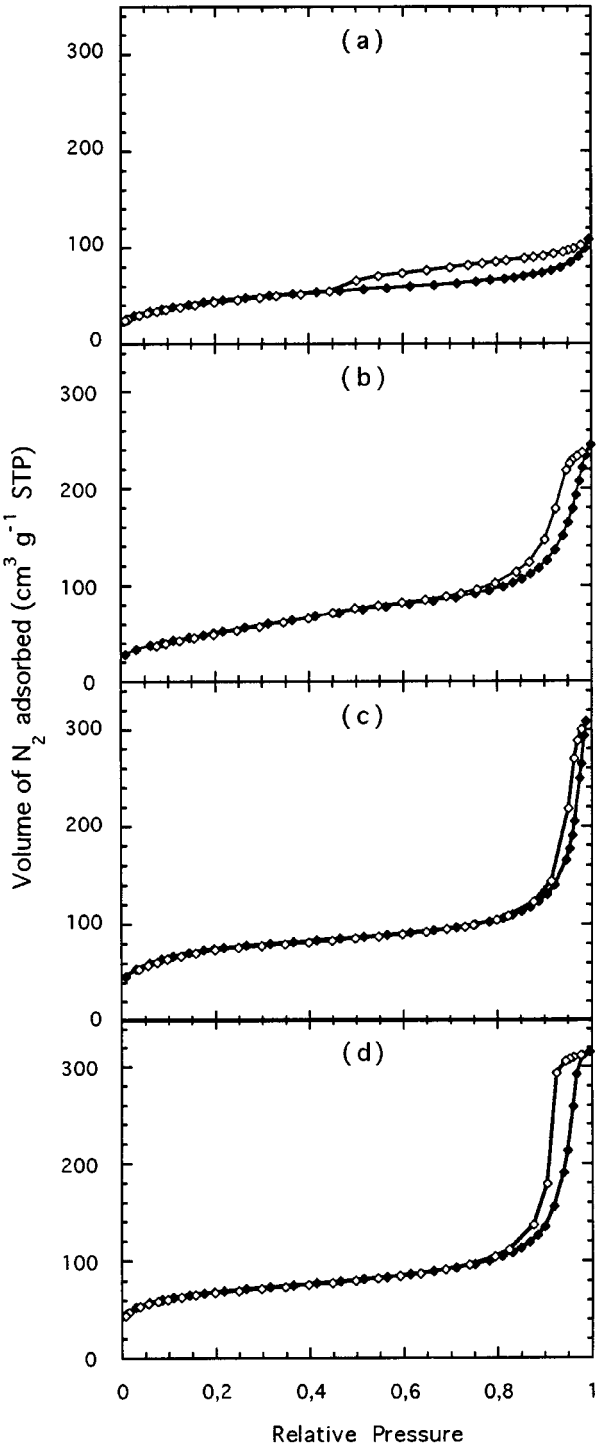


**FIG. 7.** Nitrogen adsorption–desorption isotherms at 77 K of the samples calcined at 573 K: (a) CoAl2; (b) Mg(0.25)CoAl2, (c) Mg(1)CoAl2, (d) Mg(4)CoAl2.

Moreover, a high Mg content gave rise to a significant microporous domain which maintained after calcination at 773 K. Figure 8 also provides evidence for the stabilizing role of Al since the samples with $M^{2+}/Al^{3+} = 2$ exhibit

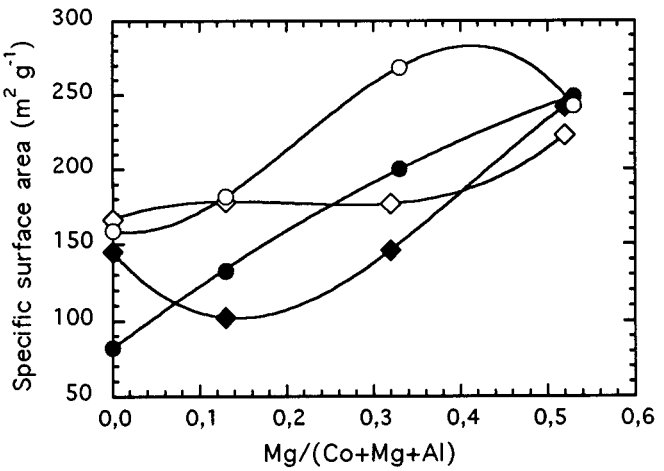


**FIG. 8.** Variation of the specific surface area of the samples with $M^{2+}/Al^{3+} = 2$ (○, ●) and $M^{2+}/Al^{3+} = 3$ (◇, ◆) calcined at 573 K (open symbols) and 773 K (closed symbols) as a function of the Mg content.

surface areas generally higher than the samples with $M^{2+}/Al^{3+} = 3$.

*Reduction of the LDHs and of the Mixed Oxides*

Figures 10 and 11 present the TPR profiles of the Co/Mg/Al samples after drying at 353 K and calcination at 623 or 773 K, respectively. The $H_2$ uptakes are listed in Table 3. As general comments, one can observe the following:

(i) For all the samples, two domains exist for the $H_2$ consumption, in the low-temperature (LT) and high-temperature (HT) ranges. In some cases, these $H_2$ consumptions

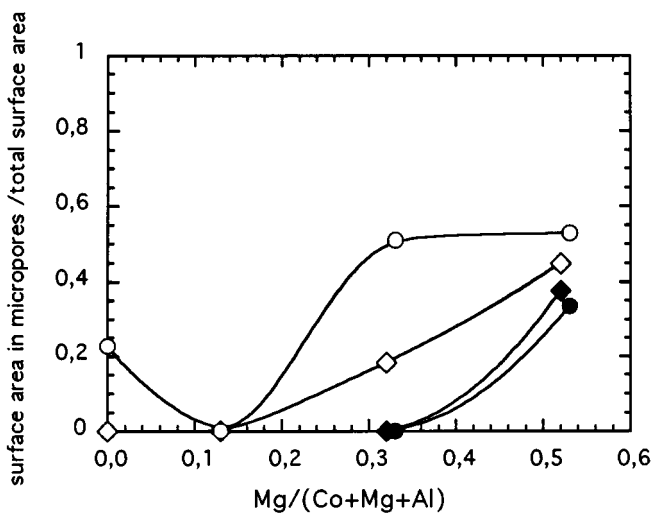


**FIG. 9.** Variation of the specific area in the micropores of the samples with $M^{2+}/Al^{3+} = 2$ (○, ●) and $M^{2+}/Al^{3+} = 3$ (◇, ◆) calcined at 573 K (open symbols) and 773 K (closed symbols) as a function of the Mg content.

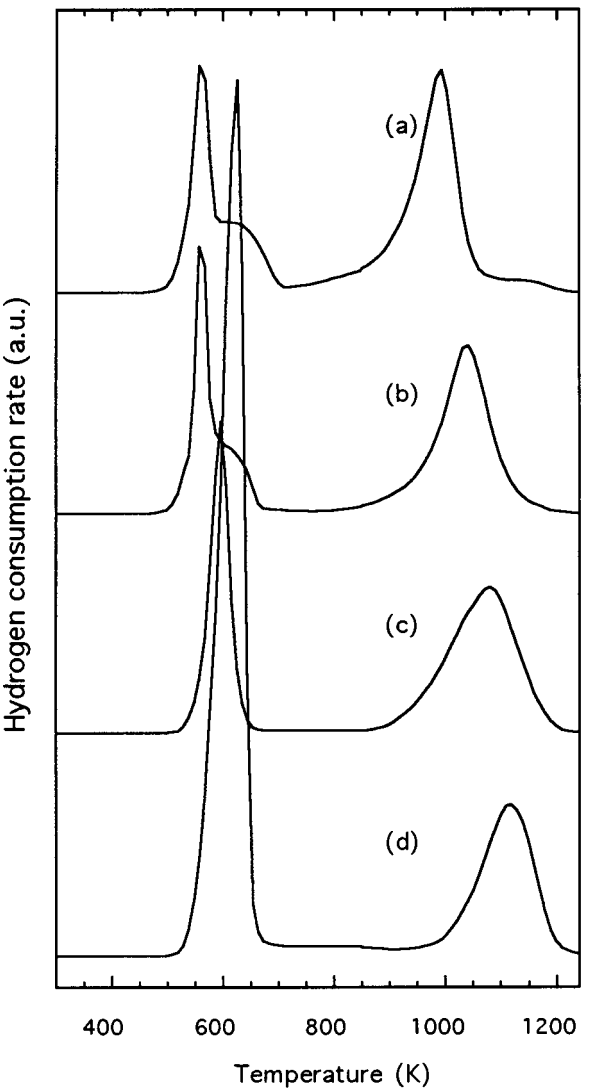


**FIG. 10.** Temperature-programmed reduction profiles of the non-calcined samples: (a) CoAl2, (b) Mg(0.25)CoAl2, (c) Mg(1)CoAl2, (d) Mg(4)CoAl2.

are featured by broad unresolved peaks with shoulders, which provide evidence of the reduction of several different cobalt species. A great number of cobalt species, in interaction with the support, were proposed in various supported cobalt catalysts (3, 5, 26). Arnoldy and Moulijn (5) thus identified up to five different species in $Co/Al_2O_3$ as a function of Co loading and calcination temperature.

(ii) $H_2$ consumption tends to decrease after calcination of the sample at 623 K and further at 773 K. This decrease, which can be higher than 50%, takes place mainly for the LT $H_2$ consumption.

(iii) There are two clear contributions in the LT $H_2$ consumption for samples with $Mg/Co < 1$, which transformed into a narrow and intense peak of $H_2$ consumption for the samples with $Mg/Co \geq 1$.

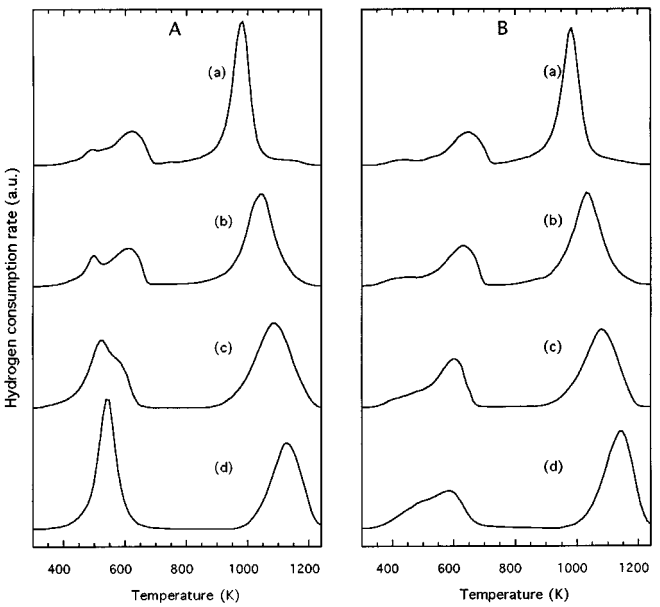


**FIG. 11.** Temperature-programmed reduction profiles of the samples calcined at 623 K (A) and 773 K (B): (a) CoAl2, (b) Mg(0.25)CoAl2, (c) Mg(1)CoAl2, (d) Mg(4)CoAl2.

(iv) There is an upward shift of the faster reduction rate, for the HT $H_2$ consumption, when the Mg content increases. Moreover, this shift is Al content dependent since it reaches ca. 80 K for the sample series with $(Mg + Co)/Al = 3$, and ca. 140 K for the series with $(Mg + Co)/Al = 2$.

With the aim of clarifying these behaviors and identifying the different contributions in the TPR profiles, the TPR of CoAl2 and Mg(4)CoAl2 were followed by mass spectrometry (Fig. 12). After drying at 353 K there was a first peak of $H_2O$ evolution below 423–473 K which corresponds to the release of interlayer water. CoAl2 exhibited then a first $H_2$ consumption at ca. 650 K with a concurrent release of $CO_2$ (mass 44), NO (mass 30), and $H_2O$ (mass 18) (Fig. 12a). The reduction of $NO_3^-$ to NO thus corresponds to the first intense peak observed in TPR profiles (Fig. 10a) at ca. 570 K. $NO_2$ was not detected due to reduction into NO. The first $H_2$ consumption was followed by a second one, which appeared as a shoulder at 750 K with a concurrent $H_2O$ evolution (Fig. 12a). This provides evidence that the reduction of some Co species has occurred which corresponds to the second $H_2$ uptake observed at 620 K in the TPR experiments (Fig. 10a). On the other hand, for Mg(4)CoAl2 the $H_2$ consumption gave, in the same temperature range, a unique and broad peak from 573 to 823 K with $CO_2$, NO, and $H_2O$ evolutions (Fig. 12c). This is in agreement with the unique and intense peak observed in TPR (Fig. 10d). For CoAl2 and Mg(4)CoAl2, which only suffered drying at 353 K, the total $H_2$ consumptions corresponds to $H_2$/Co stoichiometry larger than one (Table 3), due to the simultaneous reduction of Co and $NO_3^-$ species. The mass spectrometry profiles of CoAl2 calcined at 623 K (Fig. 12b) shows below 773 K only one broad peak of $H_2$ consumption with a concurrent $H_2O$ evolution thus attributed to the reduction of Co species. This $H_2$ uptake corresponds to the LT $H_2$ peak in the TPR experiment (Fig. 11a). Trace amounts of NO are only detected in agreement with the nearly complete decomposition of $NO_3^-$ after calcination at 623 K. The $H_2$/Co molar ratio is therefore close to one. Mg(4)CoAl2 calcined at 623 K exhibited a rather different behavior (Fig. 12d). The first $H_2$ consumption corresponds well with a still intense peak of NO evolution, while the release of $H_2O$ is shifted by 100 K at higher temperature. The reduction of remaining $NO_3^-$ explains the $H_2$/Co stoichiometry of 1.2 (Table 3), and the shift to higher values of the LT peak in the TPR profile (Fig. 11d). When Mg(4)CoAl2 was previously calcined at 773 K, only one broad peak of $H_2$ consumption with a concurrent evolution of $H_2O$ is observed in the LT range, thus corresponding to the reduction of a Co species alone (Fig. 12e). The $H_2$/Co stoichiometry is close to one (Table 3). The behavior of these samples is thus in agreement with (i) the higher thermal stability of $NO_3^-$ and $CO_3^{2-}$ at increased Mg content and (ii) the existence in the LT $H_2$ consumption domain of reducible Co species, which could be CoO or $Co_3O_4$ generally reduced in this temperature range (5). It is worth noting that for the samples calcined at high temperature, the $H_2$ consumption ratio between the LT and HT peaks increases with the Mg content. This is likely due to a different reducibility of the two Co species.

## DISCUSSION AND CONCLUSIONS

The Co/Mg/Al layered double hydroxides of this study show a unique layered structure. The evolution of the lattice *a* parameter with the composition in cations provides evidence that $Co^{2+}$, $Mg^{2+}$, and $Al^{3+}$ are combined in the same layer. However, in these syntheses performed at pH = 9, $Mg^{2+}$ is always introduced in the LDH in lower amounts than expected from the composition of the solutions. This reflects the complex nature of the coprecipitation mechanism involved when several cations are present (9). The crystallinity is dependent on the amounts of $Co^{2+}$ and/or $Mg^{2+}$, probably due to their respective ionic radius. The high stacking orders along the *c* axis, as found in the CoAl2 and CoAl3 samples, are in line with previous reports on similar LDH materials (17, 27). The isomorphous replacement of $Co^{2+}$ by $Mg^{2+}$ has three main effects:

(i) an increase in the amount of interlayer water due to the well-known ability of these cations to be hydrated (28);

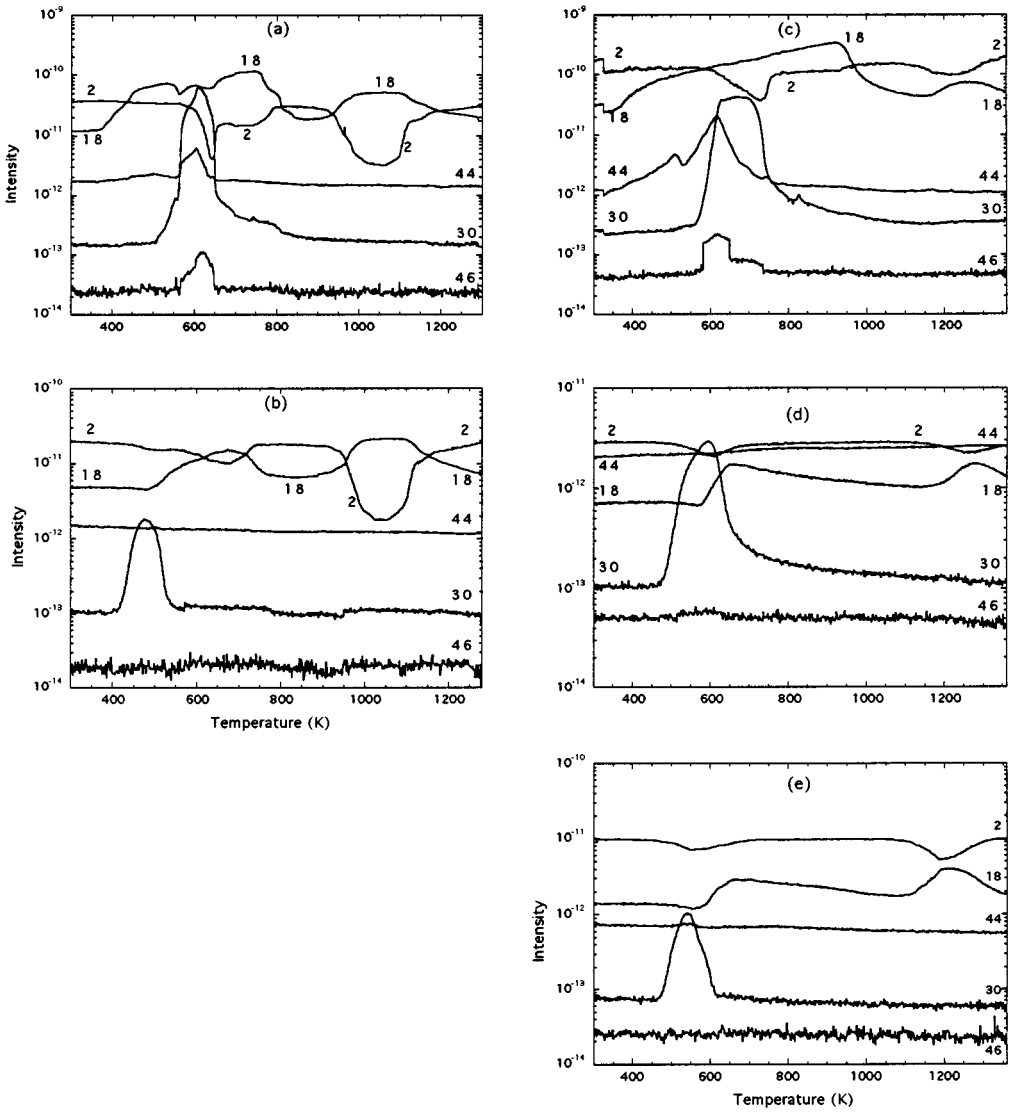


**FIG. 12.** Mass spectrometry profiles of the gases evolved during a programmed reduction of various samples; CoAl2 noncalcined (a) and calcined at 623 K (b); Mg(4)CoAl2 noncalcined (c), and calcined at 623 K (d) and at 773 K (e).

(ii) a higher thermal stability of $CO_3^{2-}$ and $NO_3^-$ shown by TG and mass spectrometry experiments due to the higher local charge density of the layers when $Co^{2+}$ is replaced by divalent cations of smaller ionic radius, or to the higher affinity of $Mg^{2+}$ for $CO_3^{2-}$ (29)—this also means that the basicity of these samples is enhanced when Mg is introduced (3);

(iii) a stabilization of the specific area—this might result from the decrease in the amount of spinel phase.

XRD studies, thermal decomposition, and TPR experiments allow us to explain the decomposition processes and to identify the crystalline phases formed in these mixed Co/Mg/Al oxides. Specific behaviors have been reported in the literature for the decomposition of different hydrotalcite-like systems. For example, the Ni/Mg/Al LDH materials are decomposed up to 1100 K into a mixed oxide of $M^{II}(Al)O$ type, where the reducibility of Ni decreases with the Mg content and the calcination temperature of the starting material (12, 20). In the case of hydrotalcite-like compounds containing copper, like Cu/Co/Al (30), Cu/Zn/Al (31), and Cu/Mg/Al (32), CuO segregates in each case. The present study confirms that the Co/Al starting materials decomposed into a spinel phase upon calcination above 573 K. A nonstoichiometric spinel phase was even detected at 473 K (17). This indicates that spinel formation is thermodynamically more favored with Co than with Mg or Ni. The latter elements give a mixed metal oxide in the same temperature range and the spinel phase only above

**TABLE 3**
**List of $H_2$ Uptakes in TPR Experiment**

| Sample | mol $H_2$/mol CO | | |
|---|---|---|---|
| | Uncalcined | 573 K | 773 K |
| CoAl2 | 1.32 | 0.85 | 1.00 |
| CoAl3 | 1.01 | 0.99 | 0.99 |
| Mg(0.25)CoAl2 | 1.08 | 0.94 | 1.08 |
| Mg(1)CoAl2 | 0.98 | 1.27 | 1.04 |
| Mg(4)CoAl2 | 1.78 | 1.26 | 1.10 |
| Mg(0.25)CoAl3 | 1.27 | 1.11 | 1.12 |
| Mg(1)CoAl3 | 1.31 | 1.27 | 1.13 |
| Mg(4)CoAl3 | 1.34 | 1.41 | 1.02 |

1073 K (2, 10). In the composite Co/Mg/Al hydrotalcites, the different crystalline phases obtained are very dependent on the chemical composition. A spinel-like phase is detected above 573 K at low Mg content, i.e., with $Co^{2+}/Mg^{2+}$ ratios of 4/1 and 1/1, respectively, but with a lower crystallinity in the latter case. The MgO-type phase is never identified in these samples within the limits of detection by XRD. In contrast, MgO is indeed identified in the Mg rich samples ($Co^{2+}/Mg^{2+} = 0.25$). One could speculate that Co and Mg segregate in distinct phases, as shown by the single separate phase in the XRD patterns. The TPR experiments provide additional informations on these multiple phases components, and at least two Co species are always detected. In these LDH compounds, Co could interact with Mg and/or Al. From the TPR studies on the reducibility of $Co/Al_2O_3$ catalysts (5) it was concluded that, besides $Al_2O_3$, two main phases are present in the temperature range investigated: $Co_3O_4$ and a $CoAl_2O_4$ spinel which reduced around 600 K and above 1100 K, respectively. In the case of $Co_3O_4$–MgO catalysts, Sexton *et al.* (26) showed that $Co_3O_4$ was first reduced to CoO which then reacted with MgO to give a solid solution; this solid solution is in turn reduced around 773–873 K. In the composite Co/Mg/Al compounds, spinel solid solutions of the type $Co_{1-x}Mg_xAl_2O_4$ have been reported and used as catalysts for $N_2O$ decomposition (18, 19) or CO oxidation (33).

On the basis of these arguments, the occurrence of $Co_3O_4$, reduced below 693 K, and of $CoAl_2O_4$ reduced around 970–1030 K, is very likely for CoAl2 and CoAl3 samples calcined at above 673 K. Their spinel structures give similar XRD patterns. The reduction of $Co_3O_4$ normally occurs in two steps, $Co_3O_4 \rightarrow CoO \rightarrow Co$ (5, 26), and the corresponding reduction peaks, both around 600 K, are almost indistinguishable (4, 5, 26). This explains the broadening of the first TPR peak assigned to $Co_3O_4$ reduction in CoAl2 and CoAl3 (Fig. 11). The total $H_2$ taken up by the reduction of these calcined samples (Table 2) is lower than expected by the occurrence of $Co_3O_4$; very likely Co species are not fully reduced. The occurrence of both $Co_3O_4$ and the stoichiometric spinel phase could easily be justified on the basis of the compositions of Mg(0.25)CoAl2 and Mg(1)CoAl2 with Co/Al values of 1.6 and 1, respectively. Moreover, an alumina phase is also expected if the same phases are formed in the Mg(4)CoAl2 sample. On the other hand, when the amount of Mg increases the main changes in the TPR profiles are as follows:

(i) an increase of the $H_2$ consumption in the first reduction peak accounting for an increasing amount of $Co_3O_4$ or for a lower size of these particles;

(ii) an increase in the reduction temperature of the second peak—this suggests that a nonstoichiometric spinel phase containing Mg is formed which decreases the reducibility of Co or that the accessibility to Co belonging to $CoAl_2O_4$ is hindered by the presence of increasing amounts of Mg(Al)O phase.

Therefore, the catalysts obtained from the LDH precursors give a $Co_3O_4$ phase easily reducible below 723 K, and Co species which reduce at higher temperature depending on the nature and the amount of the other cations in the layer. This is due to the great ability of Co to be combined in spinel-like phases, which is particularly true when the neighboring cations are Al and Mg. However, their specific surface areas and their control reducibility by the way either of the temperature or of the composition, make them available as hydrogenation catalysts.

## REFERENCES


1. H. Schulz, E. van Steen, and M. Claeys, *in* "Proceeding; 3rd Natural Gas Conversion Symposium" (H. E. Curry-Hyde and R. F. Howe, Eds.), p. 204, Stud. Surf. Sci. Catal., Vol. 81. Elsevier Amsterdam 1993.
2. J. Volf and J. Pasek, "Catalytic Hydrogenation" (L. Cerverny, Ed.), p. 105, Stud. Surf. Sci. Catal., Vol. 27. Elsevier, Amsterdam, 1986.
3. G. S. Sewell, C. T. O'Connor, and E. van Steen, *Appl. Catal.* **125,** 99 (1995).
4. G. S. Sewell, E. van Steen, and C. T. O'Connor, *Catal. Lett.* **37,** 255 (1996).
5. P. Arnoldy and J. A. Moulijn, *J. Catal.* **93,** 38 (1985).
6. E. van Steen, G. S. Sewell, R. A. Makhothe, C. Micklethwaite, H. Manstein, M. de Lange, and C. T. O'Connor, *J. Catal.* **162,** 220 (1996).
7. F. Cavani, F. Trifiro, and A. Vaccari, *Catal. Today* **11,** 173 (1991).
8. W. T. Reichle, *Chemtech*, 58 (1986).
9. A. de Roy, C. Forano, K. El Malki, and J. P. Besse, "Synthesis of Microporous Materials" (M. L. Occelli and H. Robson, Eds.), Vol. 2, p. 108. Van Nostrand–Reinhold, New York, 1992.
10. W. T. Reichle, S. Y. Kang, and D. S. Everhardt, *J. Catal.* **101,** 352 (1986).
11. A. L. McKenzie, C. T. Fishel, and R. J. Davis, *J. Catal.* **138,** 547 (1992).
12. D. Tichit, F. Medina, B. Coq, and R. Dutartre, *Appl. Catal.* **159,** 241 (1997).
13. C. De Bellefon and P. Fouilloux, *Catal Rev. Sci. Eng.* **36,** 459 (1994).
14. M. J. F. M. Verhaak, A. J. van Dillen, and J. W. Geus, *Catal. Lett.* **26,** 37 (1994).
15. N. V. Pavlenko, A. I. Tripol'skii, E. V. Prokhorenko, and G. I. Golodets, *Kinet. Katal.* **28,** 1382 (1987).

16. C. V. Rode, M. Arai, M. Shirai, and Y. Nishiyama, *Appl. Catal.* **148,** 405 (1997).
17. S. Kannan, S. Velu, V. Ramkumar, and C. S. Swamy, *J. Mater. Sci.* **30,** 1462 (1995); S. Kannan and C. S. Swamy, *J. Mater. Sci. Lett.* **11,** 1585 (1992).
18. C. Angeletti, F. Pepe, and P. Porta, *J. Chem. Soc. Faraday Trans. 1* **74,** 1595 (1978).
19. C. Angeletti, F. Pepe, and P. Porta, *J. Chem. Soc. Faraday Trans. 1* **73,** 1972 (1977).
20. O. Clause, M. Goncalves Coelho, M. Gazzano, D. Matteuzzi, F. Trifiro, and A. Vaccari, *Appl. Clay Sci.* **8,** 169 (1993).
21. F. Trifiro, A. Vaccari, and O. Clause, *Catal. Today* **21,** 185 (1994).
22. J. L. Lemaitre, "Characterization of Heterogeneous Catalysts" (F. Delaunay, Ed.), p. 34. Dekker, New York, 1984.
23. D. A. M. Monti and A. Baiker, *J. Catal.* **83,** 323 (1983).
24. M. A. Ulibarri, J. M. Fernandez, F. M. Labajos, and V. Rives, *Chem. Mater.* **3,** 626 (1991).
25. J. M. Thomas and W. J. Thomas, "Introduction to the Principles of Heterogeneous Catalysis," p. 197. Academic Press., London, 1967.
26. B. A. Sexton and A. E. Hughes, *J. Catal.* **97,** 390 (1986).
27. C. P. Kelkar and A. A. Schultz, *Microp. Mat.* **10,** 163 (1997).
28. M. K. Niemelä and A. O. I. Krause, *Catal. Lett.* **34,** 75 (1995).
29. A. Vaccari and M. Gazzano, "Preparation of Catalysts VI" (G. Poncelet, J. Martens, B. Delmon, P. A. Jacobs, and P. Grange, Eds.), p. 893, Stud. Surf. Sci. Catal., Vol. 91. Elsevier, Amsterdam, 1995.
30. A. J. Marchi, J. I. Di Cosimo, and C. R. Apesteguia, *in* "Proceedings, 9th International Congress on Catalysis" (M. J. Phillips and M. Ternan, Eds.), Vol. 2 p. 529. Chemical Institute of Canada, Ottawa, 1988.
31. C. Busetto, G. Del Piero, G. Manara, F. Trifiro, and A. Vaccari, *J. Catal.* **85,** 260 (1984).
32. I. J. Shannon, F. Rey, G. Sankar, J. M. Thomas, T. Maschmeyer, A. M. Waller, A. E. Palomares, A. Corma, A. J. Dent, and G. N. Greaves, *J. Chem. Soc. Faraday Trans.* **92,** 4331 (1996).
33. F. Pepe and M. Occhiuzzi, *J. Chem. Soc. Faraday Trans.* **90,** 905 (1994).